Experimental and Theoretical Analysis of Nanotransport in Oligophenylene Dithiol Junctions as a Function of Molecular Length and Contact Work Function

Zuoti Xie,[†,⊥] Ioan Bâldea,[*,‡,§,⊥] Christopher E. Smith,[†] Yanfei Wu,[†] and C. Daniel Frisbie[*,†]

[†]Department of Chemical Engineering and Materials Science and Department of Chemistry, University of Minnesota, Minneapolis, Minnesota 55455, United States, [‡]Theoretische Chemie, Universität Heidelberg, INF 229, D-69120 Heidelberg, Germany, and [§]National Institute of Lasers, Plasma and Radiation Physics, Institute of Space Science, POB MG-23, RO 077125 Bucharest, Romania. [⊥]Z.X. and I.B. contributed equally to this work.

ABSTRACT We report the results of an extensive investigation of metal−molecule−metal tunnel junctions based on oligophenylene dithiols (OPDs) bound to several types of electrodes (M_1−S−$(C_6H_4)_n$−S−M_2, with $1 \le n \le 4$ and $M_{1,2}$ = Ag, Au, Pt) to examine the impact of molecular length (n) and metal work function (Φ) on junction properties. Our investigation includes (1) measurements by scanning Kelvin probe microscopy of electrode work function changes ($\Delta\Phi = \Phi_{SAM} - \Phi$) caused by chemisorption of OPD self-assembled monolayers (SAMs), (2) measurements of junction current−voltage (I−V) characteristics by conducting probe atomic force microscopy in the linear and nonlinear bias ranges, and (3) direct quantitative analysis of the full I−V curves. Further, we employ transition voltage spectroscopy (TVS) to estimate the energetic alignment $\varepsilon_h = E_F - E_{HOMO}$ of the dominant molecular orbital (HOMO) relative to the Fermi energy E_F of the junction. Where photoelectron spectroscopy data are available, the ε_h values agree very well with those determined by TVS. Using a single-level model, which we justify *via ab initio* quantum chemical calculations at post-density functional theory level and additional UV−visible absorption measurements, we are able to quantitatively reproduce the I−V measurements in the whole bias range investigated (∼1.0−1.5 V) and to understand the behavior of ε_h and Γ (contact coupling strength) extracted from experiment. We find that Fermi level pinning induced by the strong dipole of the metal−S bond causes a significant shift of the HOMO energy of an adsorbed molecule, resulting in ε_h exhibiting a weak dependence with the work function Φ. Both of these parameters play a key role in determining the tunneling attenuation factor (β) and junction resistance (R). Correlation among Φ, $\Delta\Phi$, R, transition voltage (V_t), and ε_h and accurate simulation provide a remarkably complete picture of tunneling transport in these prototypical molecular junctions.

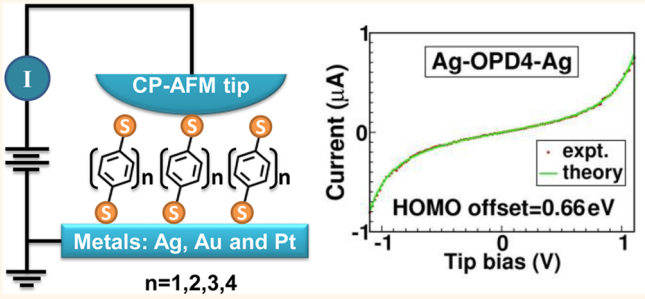

KEYWORDS: molecular electronics · molecular junctions · tunneling · charge transport · oligophenylene dithiol · work function · transport model

Molecular electronics research is driven by the potential for molecular-level engineering of electronic function in new nanodevices and by a desire for better understanding of charge transport mechanisms in molecular systems.[1−21] Over the past 15 years, one of the main challenges in molecular electronics, at least from the experimentalist's viewpoint, has been the lack of easily accessible quantitative models for the current−voltage (I−V) characteristics of molecular tunnel junctions. Conventional density functional theory (DFT) calculations, which represent the vast majority of the theoretical studies on molecular transport,[19,22−33] are able to provide important information, for example, on molecular conformation and contact topology. However, these calculations cannot be implemented by the non-expert. On the other hand, simple analytical theories such as the Simmons model for "square barrier" tunneling,[34] while relatively

* Address correspondence to ioan.baldea@pci.uni-heidelberg.de, frisbie@umn.edu.

Received for review March 16, 2015 and accepted July 18, 2015.

Published online July 18, 2015
10.1021/acsnano.5b01629

simple to understand, have been shown repeatedly to be a poor description for molecular junctions, largely because the chemical nature of the constituent molecules is not accounted for.[34−39] Indeed, the Simmons picture, if it applied, would be a rather uninteresting model for molecular electronics because the details of molecular structure are lumped into an aggregate barrier, providing no real insight into how tunnel currents can be manipulated precisely by chemistry.[35,37,39] (In addition, the Simmons model as applied to charge transport is based on a defective mathematical approximation, as shown recently.[40]) The field has needed a more accurate analytical model, accessible to experimentalists and justifiable microscopically, in which quantitative fits to the transport data allow convenient extraction of parameters such as the highest occupied molecular orbital (HOMO) (or LUMO, lowest unoccupied molecular orbital) position, the transmission efficiency, and the strength of electronic coupling to the contacts. This information can then be employed in the design of new systems with rationally tuned transport characteristics.

The model we employ here to analyze our transport data is based on a single-level (Newns−Anderson[41]) description. As discussed in detail below (see Figure 2 and the section Remarks on the Theoretical Modeling in the Supporting Information (SI)), the fact that a single molecular orbital (namely, the HOMO) dominates the charge transport through the present junctions is justified microscopically (i) *via* equation-of-motion coupled-cluster singles and doubles calculations of the lowest ionization potentials (EOM-IP-CCSD)[42,43] at post-DFT level, which represent the state-of-the-art of quantum chemistry for the molecular sizes considered; (ii) by additional UV−visible absorption experiments; and, last but not least, (iii) by direct comparison with UPS data,[44] in cases where the latter are available (cf. Table 2). Thus, the simple one-level model we employ here is not merely a convenient picture among many other off-resonant tunneling mechanisms,[15] but it is a logical choice, and we demonstrate below that it provides an excellent overall quantitative description of a variety of experiments.

Within this single-level model, a series of simple analytical formulas have been deduced recently,[45−48] which are useful to describe the off-resonant, coherent tunneling typical of the vast majority of molecular junctions. Besides the zero-bias resistance R, $\varepsilon_h = E_F - E_{HOMO}$ (the HOMO position with respect to the Fermi level E_F) is a basic quantity of this approach.[47] In a nonresonant situation (which turned out to be the case for all of our junctions), ε_h can be found straightforwardly from the minimum $V = V_t$ in a Fowler−Nordheim (F−N) plot of the same I−V characteristic. The transition voltage V_t is a characteristic voltage evident by inspection of the F−N plot that can be related analytically to ε_h (see eqs 4 and S2 and

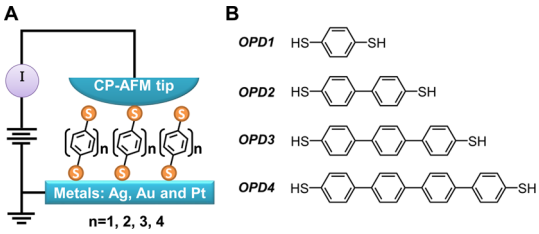

Figure 1. Schematic representation of the conducting probe atomic force microscopy setup. A metal-coated (Ag, Au, Pt) AFM tip is brought into contact with a SAM of oligophenylene dithiols of various lengths on a metal-coated substrate. The tip−SAM contact area is ∼40 nm^2.

transition voltage spectroscopy (TVS)[5,44,49,50]). This, in turn, means that, in cases (and all junctions investigated in this study belong to this category) where biases (at least slightly) above V_t can be accessed experimentally, ε_h is not needed as an adjustable parameter in the fit of the full I−V characteristics. Rather, it is determined from the F−N plot and then Γ (width parameter related to molecule−electrode couplings, cf. section Basic Working Equations) is adjusted to provide the complete fit. Agreement between theory and experiment is very good in the handful of cases addressed so far,[45−48,51] and the overall approach is appealing because it is easy to implement and yields important molecule and contact-specific electronic structure information.

In this paper, we describe an extensive experimental and theoretical investigation of a benchmark molecular electronics system, namely, oligophenylene dithiols (OPDs) between metals, as a function of molecular length (up to four phenylene rings) and contact work function (Figure 1). This work builds on previous studies by our research group of oligoacene thiols and dithiols[44,52] and alkanethiols and dithiols,[35,53−55] as well as on work done by other groups on various molecules.[1,7,30,56−66] To our knowledge, the effect of the contact work function and the related Fermi level pinning has not been addressed before for OPD junctions. Such studies, following earlier work on bond polarization at metal surfaces,[67,68] are important for OPD-based junctions; the OPD molecules have a degree of aromaticity significantly different from that of the oligoacene molecules studied in our group,[44] and the degree of pinning can vary from one molecule−electrode pair to another.

Another key difference here from our earlier work is that we are able to understand the full I−V behavior of the junctions quantitatively (up to ±1.5 V). Using the simple analytical model mentioned above and described in more detail below, we are able to extract ε_h and Γ of molecular junctions based on four different OPDs and different combinations of Ag, Au, and Pt contacts, a total of 12 distinct metal−molecule−metal junctions. The theory agrees with experiment in all cases. Our investigation (1) adds to the growing body

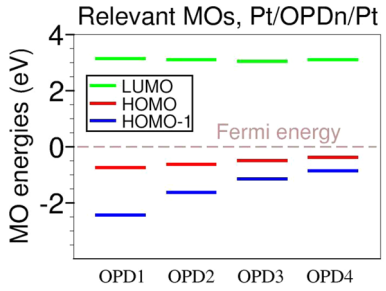

Figure 2. Microscopic justification of the single-level ("only HOMO") model used to interpret the present transport data. The diagram presents the energies of relevant molecular orbitals for Pt/OPDn/Pt junctions. The alignment of the HOMOs with respect to the metallic Fermi level are given by the ε_h values of Table 1. The energy differences between HOMO and HOMO−1 (equal to the differences between the green and red lines of Figure 8A) have been obtained *via* EOM-IP-CCSD quantum chemical calculations, and optical gaps extracted from UV−visible absorption data (Figure S5) have been utilized as estimations for the LUMO positions.

of evidence that molecular junction transport characteristics can be accurately modeled by an analytical theory; (2) provides the most comprehensive analysis yet of the OPD system; (3) confirms the important role of Fermi level pinning on the transport and electronic characteristics of molecular junctions with metal−thiolate contacts; and (4) solidifies the utility of TVS for quantitative *I*−*V* analysis. In the most general sense, we believe that the present work is an example of both the high-quality data that can be obtained for molecular tunnel junctions and the ability of theory to accurately model the results and return key transport parameters.

RESULTS AND DISCUSSION

As shown below, like in other cases,[32,46−48,51,69] the single-level model with Lorentzian transmission (also known as the Newns−Anderson model[41,70−72]) provides an appropriate framework for analyzing all the experimental data on the transport through conducting probe atomic force microscopy (CP-AFM) molecular junctions based on oligophenylene dithiols reported in this study. As already noted in the introduction, we adopt this model not because of its simplicity but rather because, for these junctions, it has a solid microscopic justification; the dominant role of the HOMO is visualized in Figure 2, which depicts the LUMOs much more distant from the Fermi energy and the (HOMO−1) orbitals are also sufficiently far away. Thus, the charge transport is described as a specific off-resonant coherent tunneling process (see also the section Remarks on the Theoretical Modeling in the SI for further details) mediated by the dominant molecular orbital, which is characterized by an energy offset $\varepsilon_h = E_F - E_{HOMO}$ relative to the electrodes' equilibrium (*i.e.*, zero-bias $V = 0$) Fermi energy E_F. Below we describe the key equations.

Basic Working Equations. In cases (like the present and other cases[32,45−48]), where the energy offset ε_h is sufficiently larger than the contact coupling strengths (also referred to as level width parameters) $\Gamma_{s,t}$ determined by the molecular coupling to the substrate (s) and tip (t) [more precisely to order $O(\Gamma_s\Gamma_t/\varepsilon_h^2)$] and for biases V not too high (say, $e|V| \lesssim 1.5\varepsilon_h$), particularly simple analytical formulas have been deduced.[47] The current I through a single molecule can be expressed

$$I_1 = G_1 V \frac{\varepsilon_h^2}{\varepsilon_h^2 - (eV/2)^2} \quad (1)$$

where the zero-bias conductance of a single molecule is given by

$$G_1 = G_0 \frac{\Gamma_s \Gamma_t}{\varepsilon_h^2} \quad (2)$$

with $G_0 = 2e^2/h = 77.48\ \mu S$ being the conductance quantum. In general, an applied bias can shift the molecular orbital energy

$$\varepsilon_h \rightarrow \varepsilon_h(V) = \varepsilon_h - \gamma eV \quad (3)$$

A nonvanishing voltage division factor γ[47,73] yields an asymmetric *I*−*V* curve [$I(V) \neq -I(-V)$], and transition voltages depend on polarity bias ($V_{t+} \neq -V_{t-}$). Because this asymmetry is insignificant for the *I*−*V* curves measured by us (see Figure 5, Figure 9, and SI Figures S8 and S10−S12, and the $V_{t\pm}$ values of Table 1), analytical formulas have been derived wherein $\gamma = 0$ can be used safely, that is, for the transition voltage $V_t = V_{t+} = -V_{t-}$[45,47] and

$$eV_t = 2\varepsilon_h/\sqrt{3} \quad (4)$$

To obtain the ε_h estimates (given in Table 1) more accurately, we employed, in fact, eq S2, which generalizes eq 4 for asymmetric cases, but γ was always found to be very small.

Equations 1, 2, and 4 refer to the transport through a *single* molecule of a given type (*i.e.*, containing a given number of phenyl rings n; the label n will be suppressed in this subsection for simplicity). If all molecules ($j = 1, 2, ..., N$ with $N \sim 100$)[54] in the bundle that constitutes a CP-AFM junction are characterized by the *same* HOMO energy offset ε_h, eq 4 still holds, while eqs 1 and 2 should be multiplied by N ($I = NI_1$, $G = NG_1$, as done in eqs 5 and 7). The current reads

$$I = V \sum_{j=1}^{N} G_{1,j} \frac{\varepsilon_{h,j}^2}{\varepsilon_{h,j}^2 - (eV/2)^2} \quad (5)$$

$$\xrightarrow{\varepsilon_{h,j} = \varepsilon_h} GV \frac{\varepsilon_h^2}{\varepsilon_h^2 - (eV/2)^2} \quad (6)$$

The zero-bias conductance G of the CP-AFM junction is given by

$$G = G_0 \sum_{j=1}^{N} \frac{\Gamma_{s,j}\Gamma_{t,j}}{\varepsilon_{h,j}^2} \xrightarrow{\varepsilon_{h,j} = \varepsilon_h} NG_0 \frac{\Gamma_{av}^2}{\varepsilon_h^2} \quad (7)$$

$$\Gamma_{av}^2 \equiv \frac{1}{N} \sum_{j=1}^{N} \Gamma_{s,j}\Gamma_{t,j} \quad (8)$$

Here Γ_{av} stands for an average width level.

TABLE 1. Summary of the Main Results for OPD CP-AFM Junctions[a]

electrode	quantity	OPD1	OPD2	OPD3	OPD4
Ag/Ag	R/R_0	6.48	25.05	145.26	794.74
$\beta = 1.56$	$V_{t+} \pm \delta V_{t+}$	1.15 ± 0.14	0.99 ± 0.07	0.85 ± 0.06	0.71 ± 0.07
	$\lvert V_{t-} \pm \delta V_{t-} \rvert$	1.15 ± 0.15	1.01 ± 0.07	0.83 ± 0.08	0.69 ± 0.06
	ε_h	1.00	0.87	0.73	0.61
	Γ_{av}	39.3	17.4	6.1	2.2
	$\Delta\Phi \pm \delta(\Delta\Phi)$	-0.06 ± 0.006	-0.12 ± 0.010	-0.12 ± 0.011	-0.15 ± 0.012
Au/Au	R/R_0	0.47	2.08	11.66	49.51
$\beta = 1.58$	$V_{t+} \pm \delta V_{t+}$	1.0 ± 0.07	0.85 ± 0.06	0.65 ± 0.08	0.55 ± 0.06
	$\lvert V_{t-} \pm \delta V_{t-} \rvert$	1.02 ± 0.07	0.83 ± 0.07	0.64 ± 0.07	0.54 ± 0.06
	ε_h	0.87	0.73	0.56	0.47
	Γ_{av}	126.9	50.6	16.4	6.7
	$\Delta\Phi \pm \delta(\Delta\Phi)$	-0.9 ± 0.005	-0.85 ± 0.005	-0.9 ± 0.007	-0.84 ± 0.009
Pt/Pt	R/R_0	0.0697	0.412	1.859	8.096
$\beta = 1.52$	$V_{t+} \pm \delta V_{t+}$	0.88 ± 0.05	0.73 ± 0.06	0.58 ± 0.07	0.44 ± 0.08
	$\lvert V_{t-} \pm \delta V_{t-} \rvert$	0.86 ± 0.06	0.73 ± 0.07	0.55 ± 0.04	0.42 ± 0.12
	ε_h	0.75	0.63	0.49	0.37
	Γ_{av}	284.1	98.2	35.9	13.0
	$\Delta\Phi \pm \delta(\Delta\Phi)$	-1.62 ± 0.013	-1.48 ± 0.009	-1.41 ± 0.007	-1.53 ± 0.011

[a] The resistance of the junctions [$R_0 \equiv h/(2e^2) = 12.9$ kΩ], transition voltages $V_{t\pm}$ in V, energies ($\varepsilon_h = -\varepsilon_0$, $\Delta\Phi$) in eV, Γ_{av} (meV) obtained from eq 7 by assuming $N = 100$. The β values are given per phenylene ring.

As we will show, the model presented here combined with our experimental measurements can be employed to obtain a comprehensive set of transport parameters for OPD junctions. Table 1 presents a summary of our main results. We will refer to this table often in the following sections, which systematically address a spectrum of issues for OPD junctions including work function effects, low-bias and high-bias transport regimes, contact resistance, Fermi level pinning, HOMO offset, and molecule-electrode coupling.

Change in Electrode Work Function ($\Delta\Phi$) Due to Adsorbed SAMs. Measured changes in the work function $\Delta\Phi$ due to adsorbed OPD SAMs are collected in Table 1 and Figure 3. As can be seen in Figure 3A,B, work function changes exhibit only a very weak dependence on the molecular length. On the other hand, $\Delta\Phi$ strongly depends on the metal; the average changes ($\Delta\Phi$) for Ag, Au, and Pt substrates are −0.11, −0.87, and −1.51 eV, respectively. These changes yield the work functions of the Φ_{SAM}-coated Ag, Au, and Pt substrates pinned to similar values. The average Φ_{SAM} values are 4.14 eV (Ag), 4.33 eV (Au), and 4.14 eV (Pt), to be compared with the metal intrinsic Φ values of 4.25 eV (Ag), 5.20 eV (Au), and 5.65 eV (Pt). The strong dependence of $\Delta\Phi$ on the type of metal is also reflected in the strong correlation between $\Delta\Phi$ and Φ revealed by our data, as shown in Figure 3C, which displays a linear dependence of $\Delta\Phi$ on Φ, with a slope of −0.97 and a correlation coefficient of 0.95.

The dependence of $\Delta\Phi$ on the type of metal is in agreement with DFT calculations,[74,75] which indicate that the magnitude of the metal−thiol bond dipole strongly depends on the metal. This suggests that the change in the work function $\Delta\Phi$ is caused by metal−S bond dipoles, and that the magnitude of the metal−S bond dipole scales almost proportionately with Φ, a finding similar to that reported earlier for oligoacene thiols.[44] The negative sign of the $\Delta\Phi$ values measured here for OPDs is also similar to the case of oligoacenes[44] and reveals a net electron donation to the metal. This again supports the picture emerging from DFT calculations,[74,75] showing that the adsorption of aromatic thiolate yields a decrease in the electron density of the aromatic C−S bond with a concomitant increase of the electron density of the metal−S bond. So, from this analysis, we conclude that the metal−S bond dipoles are mainly responsible for $\Delta\Phi$. This picture is consistent not only with previous findings on the local origin of $\Delta\Phi$[44] by photoelectron spectroscopy (suggesting that dipole layers at organic−metal interfaces could be formed within a few angstroms from the surface[76,77]) but also with a standard Helmholtz description and our quantum chemical calculations, which we present next.

Within the usual picture,[78] chemisorbed OPD SAMs are modeled as two effective dipole sheets: a layer characterized by the dipole moment of the adsorbate (OPD) and another layer characterized by the dipole moment of the metal−sulfur unit (normal components $\mu^{\perp}_{OPDn}$ and $\mu^{\perp}_{M-S}$). The change in the work function obtained within this picture based on classical electrostatics is[78]

$$\Delta\Phi = -\frac{N}{\mathcal{A}}\frac{e}{\varepsilon_0}\left(\frac{\mu^{\perp}_{OPDn}}{\kappa_{OPDn}} + \frac{\mu^{\perp}_{M-S}}{\kappa_{M-S}}\right) \qquad (9)$$

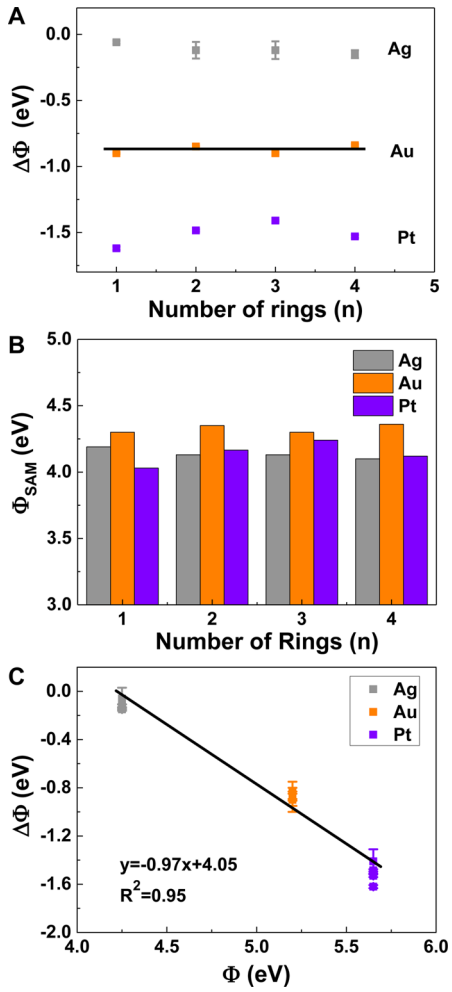

Figure 3. (A) Change in the work function ($\Delta\Phi_n = \Phi_{SAM,n} - \Phi$), due to OPD ($n$ = 1, 2, 3, and 4) SAM adsorption. (B) Work function $\Phi_{SAM,n}$ of metallic (Ag, Au, and Pt) surfaces with adsorbed OPD SAMs. (C) $\Delta\Phi_n = (\Phi_{SAM,n} - \Phi)$ *versus* bulk metal work function Φ.

Here ε_0 is the vacuum permittivity, κ_{OPDn} and κ_{M-S} are the corresponding effective dielectric constants, and $N/\mathcal{A}$ denotes the number of molecules per unit area. Due to their C_i symmetry, the dipole moment of the isolated OPD1 and OPD3 molecules vanishes. The isolated OPD2 and OPD4 molecules possess nonvanishing dipole moments. Our DFT calculations yielded nearly equal values μ_{OPD2} = 1.65 D and μ_{OPD4} = 1.64 D. However, due to their C_2 symmetry, their dipole moments are perpendicular to the molecular axis. Because the molecular axis is almost normal to electrodes' surface ($\mu^{\perp}_{OPDn} = \mu_{OPDn} \sin\varphi \simeq 0$, cf. Figure S2B and the small φ values given in SI), the first term in the parentheses entering eq 9 (practically) vanishes. The fact that this term is negligible explains why the experimental $\Delta\Phi$ values do not notably depend on the molecular size n (cf. Table 1 and Figure 3A) and supports the idea that $\Delta\Phi$ primarily originates from dipoles localized at the metal−S contacts rather than from the intrinsic molecular dipoles. The fact that the magnitude and even the sign of $\Delta\Phi$ substantially depend on the type of metal traces back to specific character of the charge transfer between the sulfur atom and the contacting metal.

Charge Transport: Low-Bias Range (V up to ±0.1 V). We switch now to the transport results. Detailed separate analysis and discussion of the low- and high-voltage ranges follow below. Our results for the low-bias resistance are presented in Figure 4. In discussing these results, we will separately consider the impact of the backbone (the molecular size n) and the contacts. The low-bias resistance $R_n \equiv R_{OPDn} = R$ will be analyzed by resorting to the factorization scheme[35,44,53,54]

$$R_n = R_c \exp(\beta n) \qquad (10)$$

which is convenient because it disentangles the length (exponential) dependence from the effective contact contribution R_c. It is a general feature of nonresonant tunneling, which characterizes all our junctions. It is worth noting that our transport data exhibit neither (Arrhenius) temperature dependence nor crossover to an R_n linearly dependent on n; a crossover from (nonresonant) tunneling to conduction *via* hopping can only be expected at larger sizes.[5,15,79−81] From the slope of the semilogarithmic plot of $R = R_n$ *versus* molecular size n, one can determine the tunneling attenuation factor β, and its intercept at n = 0 gives the effective contact resistance R_c.

Tunneling Attenuation Factor, β. Figure 4A displays a semilog plot of resistance *versus* number of phenyl rings for OPD junctions. Resistances were calculated from the average of about 150−250 I−V traces within ±0.1 V. The linear relationships in this figure indicate that the data are well explained within the nonresonant tunneling picture underlying eq 10. Within experimental uncertainties, the β values found here are independent of metal work functions, as reported previously.[35,44,82,83] This implies that the difference of the HOMO energy offsets ("barriers" for charge transport) caused by the different contact metals is not significant enough to vary the β values. Indeed, the pinning effect that appears in other conjugated oligoacenes[44] is also found in this case, as will be clarified below. The average value determined from the slopes of the semilog plots of Figure 4A is β = 1.58/ring = 0.37 Å^{-1}. Previous studies of CP-AFM junctions based on oligophenylene *mono*thiols and metallic electrodes found values of β = 0.41−0.61 Å^{-1}.[36,84] The present result for β is in line with the fact that, unlike in the case of saturated (*e.g.*, alkane) backbones (β values for alkane mono- and dithiols do not differ[35]), β values for CP-AFM junctions based on conjugated backbones with two thiol anchoring groups are smaller than those of monothiols. For the higher conjugated oligoacenes, the β values are 0.2 and 0.5 Å^{-1} for dithiols and monothiols, respectively.[44] So, the present finding indicates that, for molecules with delocalized electrons, β is not only a backbone

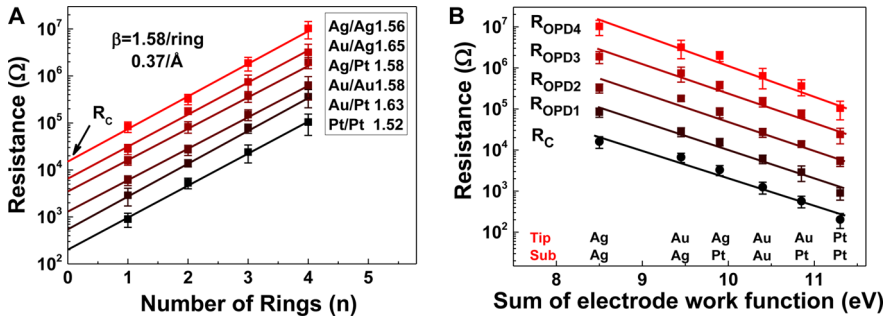

Figure 4. (A) Semilog plot of low-bias resistance *versus* number of phenyl rings (*n*). The inset shows the coated tip/substrate metals and the respective β values of each junction. (B) Semilog plot of molecular resistance (R_{OPDn}, n = 1, 2, 3, and 4) and contact resistance (R_c) *versus* the sum of the work functions of the two electrodes.

property, as it also depends on the number of thiol contacting groups.[44]

Contact Resistance *versus* Metal Work Function. The contact resistance R_c determined from the zero length intercept clearly indicates the important role of the type of electrodes. As shown in Table S2 and Figure 4B, the bare electrode work function Φ has a dramatic effect on the contact resistance R_c (and implicitly on R_{OPDn}). For the electrodes studied (Ag, Au, and Pt), Φ increases by 1.4 eV, and this manifests itself in (contact) resistance decreasing by a factor of ~70. As noted earlier, the opposite variations in Φ and R reveal a hole (p-type, HOMO-mediated) conduction. This dramatic decrease in R_c with Φ for oligophenylene dithiol junctions is comparable to that of our previous studies on alkane dithiol- and oligoacene dithiol-based CP-AFM junctions.[35,44] For monothiol-based junctions of alkanes or oligoacenes and the same electrodes as those used here, the decrease in R_c is even larger (by about 3 orders of magnitude).[35,44,55] However, no significant β value changes were found in those previous results. This indicates that the β values are much less sensitive to the level alignment than the effective contact resistance in those junctions.

General *I*−*V* Behavior. Figure 5 and Figure S8 display representative *I*−*V* characteristics of our CP-AFM junctions based on OPDs and various metallic electrodes (s, t = Ag, Au, or Pt). *I*−*V* traces are nearly symmetric with respect to the origin and exhibit a nonlinearity that becomes more pronounced at higher biases. For a given bias, the current decreases exponentially with the length. The currents for junctions based on a given molecular species (OPD) increase as the electrodes' work function increases. These attributes indicate hole (HOMO-mediated) conduction and a nonresonant tunneling mechanism. As evidence of the unipolar conduction (mediated by HOMO and negligible LUMO contribution, Figure 2), we refer to the UV−visible absorption measurements (Figure S5). Indeed, the values found for the optical gap (3.5−3.9 eV) and the HOMO energy offsets ε_h (at most 1 eV below the Fermi level, cf. Table 1) yield a LUMO located substantially higher above the Fermi level. It is worth emphasizing here that the LUMO positions depicted in Figure 2 are rather crude estimations; nevertheless, they illustrate the fact that the LUMOs are significantly more distant from the Fermi level than the HOMOs, in agreement with the various consistency tests done across the paper, which support the p-type conduction in our OPD junctions. One should still note that, as shown recently, because the exciton binding energy is substantial at the molecular sizes considered,[85] the transport HOMO−LUMO gap is larger than the optical HOMO−LUMO gap; that is, the relevant LUMO energies are even higher than that shown in Figures 2 and S7.

Nonlinear Bias Range ($|V|$ > 0.1 V): TVS and Analysis of the HOMO Energy Offset. In the analysis of the nonlinear transport, we pay special attention to the transition voltage V_t that our group proposed a few years ago.[49] V_t is the key quantity of so-called TVS. Due to its simplicity and reproducibility, a series of groups have utilized TVS as a tool for quantifying the molecular orbital energy offset relative to the electrodes' Fermi energy.[5,32,47,48,50,56−58,69,86−92] The transition voltage, defined as the bias at the minimum of the Fowler−Nordheim quantity $\ln(I/V^2)$,[49] quantifies the *I*−*V* nonlinearity: it corresponds to the point where the differential conductance is 2 times larger than the pseudo-ohmic conductance.[93]

$$\left.\frac{\partial I}{\partial V}\right|_{V=V_t} = 2\left.\frac{I}{V}\right|_{V=V_t} \qquad (11)$$

Typical TVS spectra of the oligophenylene dithiol junctions are obtained by recasting the measured *I*−*V* curves of Figure 5A,C,E in F−N coordinates $\ln(I/V^2)$ *versus* $1/V$, as depicted in Figure 5B,D,F. These F−N plots exhibit well-defined minima, which are (practically) symmetric with respect to the bias polarity ($V_t = V_{t+} \simeq -V_{t-}$). Based on eq S1, the V_t symmetry with respect to bias polarity reversal indicates that $\gamma \approx 0$ and *via* eq 3 that the applied voltage does not notably shift the HOMO energy.

The experimental results for V_t are collected in Table 1 and visualized in Figure 6. The values of the

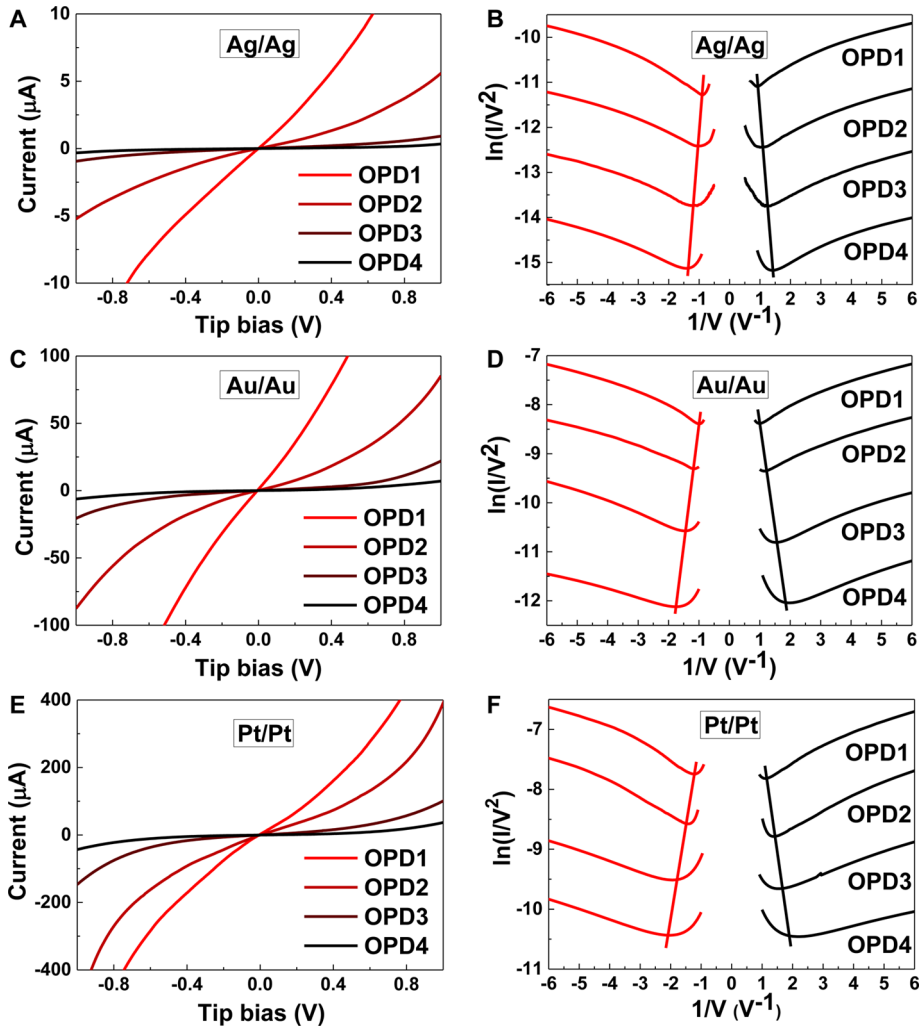

Figure 5. Representative *I*−*V* and transition voltage (ln(*I*/*V*^{2}) *vs* 1/*V*) spectra obtained by averaging 25 *I*−*V* traces for (A,B) Ag−OPD*n*−Ag, (C,D) Au−OPD*n*−Au, and (E,F) Pt−OPD*n*−Pt CP-AFM junctions. Transition voltages (V_t) are indicated by lines joining the minima.

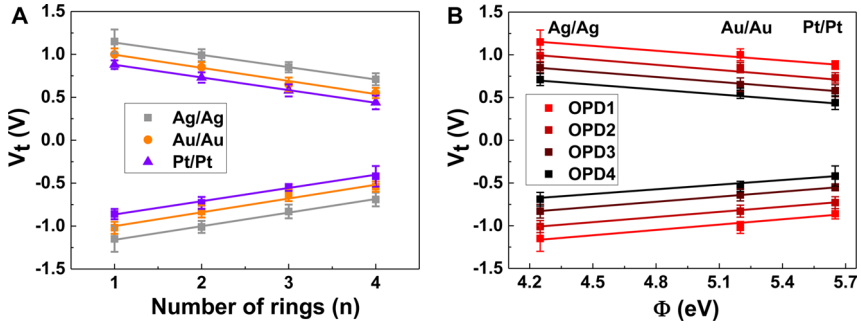

Figure 6. Transition voltages $V_{t\pm}$ of metal M−OPD*n*−M junctions (M = Ag, Au, Pt) as a function of (A) molecular length and (B) bare electrode work function.

HOMO energy offset ε_h deduced from the experimental V_t data *via* TVS (eq 4) are also included in Table 1 and Figure 7. The fact that the theoretical model employed, which underlines eq 4, is able to reproduce the measured *I*−*V* curves (see below) makes us confident of the TVS-based estimates for ε_h (see also the discussion of section Remarks on the Theoretical Modeling of Transport in the SI). As further support, it is worth noting that, for all M−OPD1−M junctions investigated here (M = Ag, Au, Pt), the present TVS-based estimates agree very well with the values directly measured by UPS[44] (see Table 2). Because the UPS and CP-AFM setups are not equivalent (one metallic contact *vs* two metallic contacts, respectively), a difference between the corresponding ε_h values may exist. To check whether this difference is significant, we have performed EOM-IP-CCSD

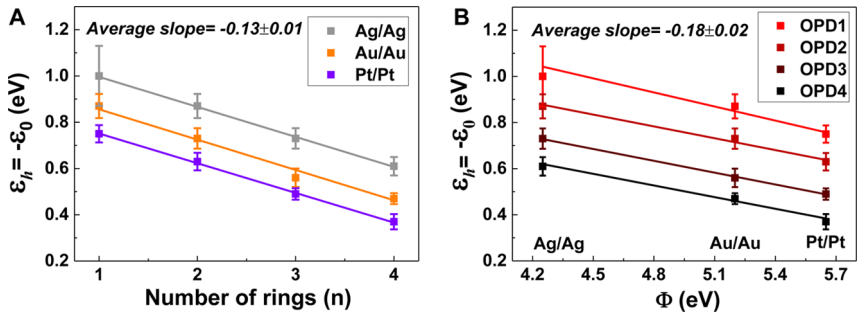

Figure 7. HOMO energy offset $\varepsilon_0 = E_{HOMO} - E_F$ deduced *via* TVS for OPD molecules embedded in metal CP-AFM junctions as a function of (A) molecular length and (B) electrode work function Φ.

TABLE 2. Values (in eV) of HOMO Energy Offsets $\varepsilon_h = E_F - E_{HOMO}$ of OPD1 and Different Metals Deduced in the Present Work *via* TVS and Direct UPS Data[a]

method	Ag	Au	Pt
TVS	1.0 ± 0.13	0.88 ± 0.05	0.75 ± 0.04
UPS	1.1	0.9	0.8

[a] Compare Table 1 of ref 44, noting that OPD1 is denoted as $Ph(SH)_2$ there.

calculations for an OPD1 molecule having gold atoms covalently bonded to one (Au−OPD1) or two (Au−OPD1−Au) thiol groups; the lowest ionization energies were found to differ only by 80 meV.

Based on Φ_{SAM} (scanning Kelvin probe microscopy, SKPM), the optical band gap (UV−visible), and ε_h obtained from eq 4, the energy-level alignments for OPD SAMs on Ag, Au, and Pt are well-defined (see Figure S7), which is essential for understanding the charge transport properties in molecular junctions.

As already encountered for other aromatic molecules,[5,44,50,86,87] we found that V_t decreases with increasing number of phenyl rings *n* (see Figure 6A). This implies *via* eq 4 a HOMO closer to the Fermi level with increasing *n*, as depicted in Figure 7A. This is related to the decrease in the optical gap observed in UV−visible absorption and is also typical of other aromatic systems.[5,44,79] As shown in Figure S5, UV−visible absorption measurements for OPD*n* confirm the decrease of the optical gap with increasing size *n*. The fact that absolute values of V_t and ε_h decrease as the electrode work function Φ increases (cf. Figure 6B and Figure 7B) is of course another indication that the charge transport through OPD*n* is mediated by the HOMO. For electromigrated benzene dithiol (OPD1) junctions, the p-type HOMO-mediated conduction has been demonstrated by electrostatic gating.[56] Because of the linear correlation between ΔΦ and Φ, we are able to plot the linear correlations of ln *R*, V_t, and ε_h *versus* ΔΦ (Figure S9).

To end this section, we briefly compare our present results for Au−OPD−Au junctions with existing reports in the literature.[56−60] Here, it is important to distinguish between the magnitude of the currents (conductances) and the transition voltages. The currents measured by us are up to 2 orders of magnitude larger than those found for electromigrated junctions[56] and STM junctions.[57−60] Basically, this difference reflects the larger number of molecules (∼100 in our CP-AFM junctions). By contrast, the present values of V_t are consistent with those deduced for electromigrated BDT ≡ OPD1 (V_t = 1.14 ± 0.04 V)[56] and STM biphenyl ≡ OPD2 (V_t = 0.91 ± 0.031 V).[58] These values agree well with the corresponding values V_t = 1.02 ± 0.07 V and V_t = 0.84 ± 0.07 V of Table 1. On this basis, we can reiterate a statement made earlier:[44,48] much more than the (low-bias) conductance, the transition voltage does represent a molecular signature.

Let us further elaborate on this point. We have just mentioned that, in contrast to the similar values of the transition voltage V_t (which are indistinguishable within experimental errors), the low-bias conductance exhibits a significant dependence on the experimental platform (CP-AFM, STM, electromigration). The interpretation of this behavior, which fits the present theoretical framework, follows. The (HOMO) widths Γ are setup-dependent (they are determined by the molecule−electrode couplings, cf. eq 13), and this makes the low-bias conductance *G* platform-dependent (cf. eqs 2 and 7). However, as long as Γ remains smaller than the HOMO offset ε_h (*i.e.*, nonresonant tunneling limit), Γ does not affect V_t, which is only determined by ε_h, as expressed by eq 4. (Remember that eq 4 and SI eqs S1 and S2 are deduced *just* by assuming $\Gamma \ll \varepsilon_h$, cf. ref 47.) So, similar V_t values imply that, at least for OPD junctions, the level alignment ε_h is weakly affected by the experimental platform. (Notice that Table 1 shows that condition $\Gamma \ll \varepsilon_h$ holds for the CP-AFM platform, despite *G* being larger than for the other two aforementioned platforms.) In fact, this is an important reason why charge transport across different molecular platforms can be very similar, as expressed by the universal behavior ("law of corresponding states") recently reported by our group;[93] irrespective of the experimental platform, in many junctions, charge tunneling is mediated by a *single off-resonant* level. Deviations from this universality (hence also platform dependence) may occur in

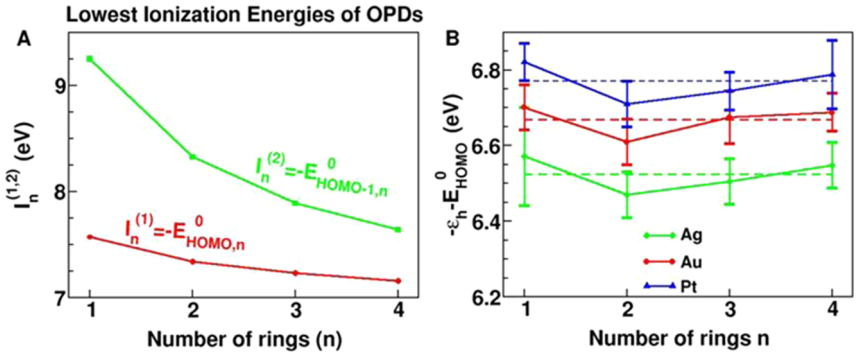

Figure 8. (A) First two ionization energies of the isolated OPD molecules computed within EOM-IP-CCSD. (B) Quantity $-\varepsilon_{h,n} - E^0_{HOMO,n} = -\varepsilon_{h,n} + I_n^{(1)}$ is independent of the molecular size n within errors. The lines are a guide for the eye.

situations close to resonance, which violate the condition $\Gamma \ll \varepsilon_h$, which underlines eq 4.

Fermi Level Pinning. Pinning of the Fermi level in molecular junctions is still somewhat underappreciated, although it was previously discussed in organic electronics[94−96] and in molecular electronics in earlier works.[28,29,44,66,97]

The slope of 0.18 obtained from a linear fit to the data in Figure 7B indicates the strong pinning of the HOMO level with respect to the metal; that is, the HOMO−Fermi offset could be tuned by the work function of the electrodes; however, this tuning is very weak; there is a 0.27 eV change in ε_h upon a 1.4 eV span in work function of the bare metals. This is consistent with our previous findings by UPS on other oligoacene molecules.[44] We ascribe this strong effect to the Fermi level pinning that was observed in our previous metal−molecule−metal junctions.[44]

To further quantify the effect of the electrodes, we next consider the difference between the HOMO energy of an OPD molecule embedded in a junction $E_{HOMO,n} = E_F - \varepsilon_{h,n}$ and the HOMO energy of the isolated molecule $E^0_{HOMO,n}$. The results of the quantum chemical calculations (see also the Methods section and the Supporting Information) presented in Figure 8A demonstrate that $E^0_{HOMO,n} = -I_n^{(1)}$ exhibits across the molecular series the same trend as the energy offset $\varepsilon_{h,n}$ deduced *via* TVS for the molecules embedded into CP-AFM junctions. The difference between lowest ionization potential $I_n^{(1)} = E^0_{HOMO,n}$ of the smallest (OPD1) and the largest (OPD4) isolated molecules is $\Delta I \equiv I_0^{(1)}|_{n=1} - I_0^{(1)}|_{n=4} = 0.41$ eV. This value agrees with the corresponding differences of the HOMO energy offset $\Delta\varepsilon_h \equiv \varepsilon_h|_{n=1} - \varepsilon_h|_{n=4}$ computed *via* TVS by means of eq 4; the latter values deduced from Table 1 for the electrodes utilized are $\Delta\varepsilon_h|_{Ag} = 0.39$ eV, $\Delta\varepsilon_h|_{Au} = 0.40$ eV, and $\Delta\varepsilon_h|_{Pt} = 0.38$ eV. More quantitatively, Figure 8B shows that the quantity $-\varepsilon_{h,n} - E^0_{HOMO,n}$ does not depend on n within V_t errors for all the three types of the metal we have used. The metal contact does not influence the molecular orbital trends with length. We can interpret this as the Fermi level pinning effect being primarily induced by the dipoles localized at the metal−S contacts rather than from the intrinsic molecular dipoles. This metal−S bond dipole is also independent of the length of the molecule (Figure 3B). Thus, we can conclude that the nature of the Fermi level pinning effect is reflected in two aspects: the HOMO−Fermi offset of the molecule weakly varies with the work function of the contact metals, and the molecular orbital trends with length are not changed by a fixed metal contact.

Contact Coupling Strength. With the values of $G_1 = 1/(RN)$ and ε_h from Table 1, we have determined the average level width (cf. eq 7)

$$\Gamma_{av} = \sqrt{\Gamma_s\Gamma_t} = \varepsilon_h\sqrt{G_1/G_0} \tag{12}$$

by using a value $N = 100$ estimated *via* contact mechanics, similar to earlier studies.[54] The numerical values of $\Gamma_{av} \rightarrow \Gamma_{av;n}$ for all molecular sizes n and metals considered are also included in Table 1.

In microscopic terms underlying our transport model, the coupling strengths can be expressed as[98]

$$\Gamma_{s,t;n} = \rho_{s,t}(E_F)t_{s,t;n}^2 \tag{13}$$

where $\rho_{s,t}(E_F)$ is the electrodes' density of states at the Fermi energy and $t_{s,t;n}$ are transfer (also called hopping or resonance) integrals. The latter quantify the efficiency of charge transfer between electrodes and the OPDn's HOMO. The exponential falloff of Γ_{av} with increasing n visible in Figure 9A (as well as Figure 4A, cf. eqs 7, 12, 13, and 10) traces back to the exponential falloff of the transfer integrals with distance (x), which is familiar from molecular physics[99] ($2\tau \approx \beta$)

$$t_{s,t;n} \rightarrow t_{s,t;n}(x_{s,t}) \propto \exp(-\tau x_{s,t}) \xrightarrow{x_s + x_t = n} \Gamma_{av;n}^2$$
$$= \Gamma_c^2\exp(-2\tau n) \tag{14}$$

Junctions with higher contact resistance have smaller coupling strengths ($R_c \propto \Gamma_c^{-2}$), that is, weaker HOMO−electrode couplings. The higher the work function, the closer the HOMO is to the Fermi level and the stronger the molecule−electrodes couplings (cf. Figure 9B).

Simulation of *I*−*V* Curves. As often emphasized in recent work,[5,32,47−50,56−58,79,80,86,89,90,100−103] studies beyond the linear bias range are required for

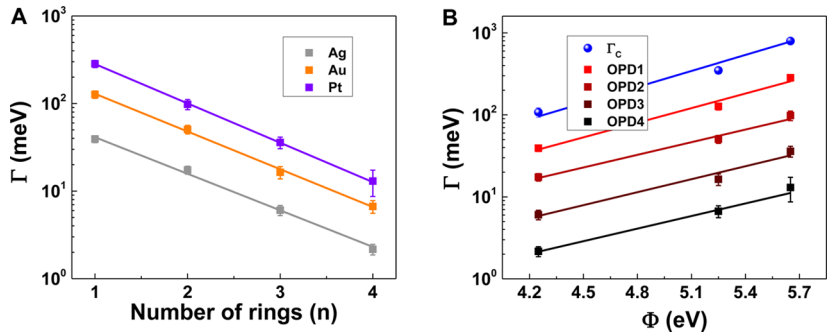

Figure 9. Average level width $\Gamma = \Gamma_{av}$ as a function of (A) molecular length *n* and (B) bare electrode work function Φ. The lines represent linear fits.

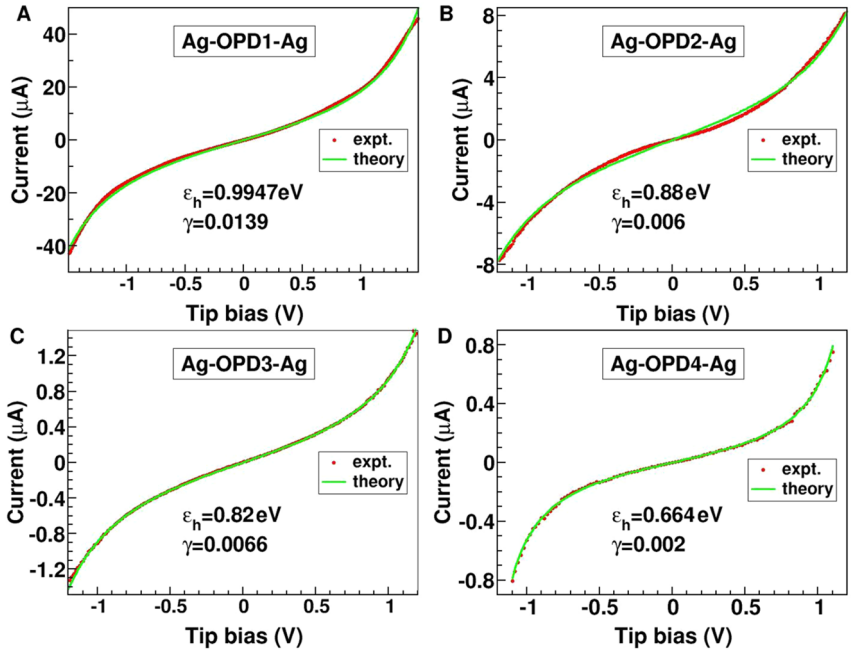

Figure 10. Agreement between the individual experimental *I*−*V* curves and those obtained theoretically *via* eq 6 is illustrated here for Ag−OPD*n*−Ag junctions.

understanding the microscopic model of charge transport through molecular devices. As is usually the case, all the *I*−*V* curves measured for OPD junctions exhibited the well-known shape, practically linear at low biases and gradually more nonlinear at higher voltages; see Figure 5.

We have checked that, maybe with one exception (shown in Figure S12 and discussed below), eq 6 reproduces very well the individual *I*−*V* curves measured for our CP-AFM junctions based on OPDs. Examples are shown in Figure 10 and SI Figures S10 and S11, where the theoretical curves are depicted in green. The parameters *G* and ε_h entering eq 6 can be determined in two ways: (i) by considering them as fitting parameters to reproduce the measured *I*−*V* curves or (ii) by extracting G_1 from the slope of the linear low-bias part of the experimental *I*−*V* curve ($|V| <$ 0.1 V) and using eq 4 (which is a direct consequence of eq 1)[47] to compute ε_h from the transition voltage V_t directly extracted from the minimum of the F−N quantity $\ln(I/V^2)$ by using the measured *I*−*V* data. We did not find notable differences between these two procedures.

The agreement between theory and experiment for the *I*−*V* curves demonstrates that the HOMO energy offsets ε_h of the bundle of molecules forming a CP-AFM junction of a given molecular species do not notably fluctuate. If the contrary were true, and eq 5 rather than eq 6 would apply, a substantial dispersion in $\varepsilon_{h,j}$ values would certainly deteriorate the agreement between the measurements and eq 6.

A Possible Special Case: Pt−OPD4−Pt. Although not dramatically large, we found certain systematic differences between eq 6 and the *I*−*V* curves measured for OPD4-based junctions and Pt electrodes; representative examples are shown in Figure S12. The fact that the relative V_t dispersion for these junctions, with the concomitantly larger spread in ε_h values, is somewhat

larger than for the other junctions (cf. Table 1) may indicate that, rather than eq 6, eq 5 applies in this case. Another conceivable source of these "discrepancies" is suggested by Figure 2 and Figure 8A. As the molecular size n becomes larger, the second ionization energy ($I_n^{(2)} \approx -E^0_{\mathrm{HOMO}-1,n}$) decreases with n faster than the first ionization energy ($I_n^{(1)} \approx -E^0_{\mathrm{HOMO},n}$) and becomes closer to it. For OPD4, the energy separation between these two ionization energies becomes comparable to the HOMO energy offset, and so one can expect an extra contribution to the charge transport from HOMO−1, which acts as a correction not included in the single (HOMO) level in the Newns−Anderson model underlying eq 6. Finally, we also mention possible reorganization effects; OPD4 is a molecule with three floppy vibrational degrees of freedom related to the three twisting angles of the relative rotations of the phenyl units. Studying the impact of reorganization of these floppy modes may be of interest, as revealed by the recent studies on bipyridine,[51,71,72] although that molecule possesses only one floppy mode.

CONCLUSION

In this paper, we have reported the results of an extensive investigation into transport and transport-related properties of oligophenylene dithiol molecules embedded in CP-AFM metal−molecule−metal junctions. Utilizing molecular species with up to n = 4 phenyl rings and electrodes of metals (Ag, Au, and Pt) having work functions Φ varying across a broad range of ∼1.4 eV, we were able to study the impact of n and Φ on relevant junction properties.

Charge transport occurs *via* nonresonant tunneling, as indicated by the exponential increase with n of the low-bias resistance R, the property most strongly affected by the molecular length. The impact of n on the change in metal work functions ($\Delta\Phi$) due to adsorbed SAMs is negligible. More strongly affected by n are optical gaps, transition voltages $V_t = V_{t+} \simeq -V_{t-}$, and HOMO energy offsets ε_h, which exhibit a roughly linear decrease also characteristic of other aromatic species. Accurate *ab initio* quantum chemical calculations allowed us to demonstrate that ε_h deduced *via* TVS (cf. eq 4) is correlated with the lowest ionization energy of isolated OPD molecules. This is evidence for a hole (HOMO-mediated) mode of conduction.

We find that β is independent of Φ due to the dominance of Fermi level pinning to the molecular HOMO levels by metal−S bond polarization. Except for the tunneling attenuation factor β, we found a pronounced impact of Φ on all the other properties investigated. While the molecular resistance $R_{\mathrm{OPD}n}$ and contact resistances R_c, which are most affected, exhibit an exponential Φ dependence, the chemisorption-induced work function change ($\Delta\Phi$), transition voltages V_t, and HOMO energy offsets ε_h are linearly correlated with Φ. The fact that increasing Φ yields a decrease in R_c and $V_t(\propto\varepsilon_h)$ is further evidence for HOMO-mediated conduction.

The relation $\varepsilon_h \propto V_t$ follows from eq 4, a result deduced within the Newns−Anderson model. By comparison of our results to appropriate UPS data available in the literature, we showed remarkably good agreement of the HOMO position with the TVS-based ε_h estimates. Furthermore, using the estimated ε_h *via* TVS and measured low-bias resistance, we were able to reproduce all the $I-V$ curves from CP-AFM measurements. This quantitative description of charge transport in CP-AFM junctions allowed us to extract a broad spectrum of valuable molecular information, and eqs 4 and 6, which underlie this method and solidify the Newns−Anderson-based TVS approach, appear to be a valuable framework for quantitative analysis in molecular electronics.

METHODS

Materials. Gold nuggets (99.999% pure) were purchased from Mowrey, Inc. (St. Paul, MN). Silver pellets (99.99% pure) were purchased from Kurt J. Lesker Company. Evaporation boats and chromium evaporation rods were purchased from R.D. Mathis (Long Beach, CA). Platinum and titanium for e-beam evaporation were purchased from Kamis, Inc. (Mahopac Falls, NY). Silicon (100) wafers were obtained from WaferNet (San Jose, CA). Contact mode AFM tips (DNP 10 silicon nitride probes) were purchased from Bruker AFM Probes. The benzene-1,4-dithiol (OPD1) 99% and *p*-terphenyl-4,4″-dithiol (OPD3) 96% used in this study were purchased from Sigma-Aldrich Company, and biphenyl-4,4′-dithiol (OPD2) 95% was purchased from TCI America. Details of the synthesis of OPD4 are provided in Supporting Information (Figure S1). Throughout, label S for equations, figures, and tables refers to the SI.

Conducting Tip and Substrate Preparation. Contact mode AFM tips were coated by Au or Ag at base pressure (<10^{-6} Torr) using a home-built thermal evaporator placed in a N_2-filled glovebox (H_2O, O_2 < 0.1 ppm). Films were deposited to a thickness of 500 Å at a rate of 0.5−1.0 Å/s atop a 50 Å Cr adhesion layer. They were immediately transferred without exposure to air to another glovebox containing the CP-AFM to carry out the $I-V$ measurements. Pt films (300 Å thick) were deposited with an e-beam evaporator with a 50 Å Ti adhesion layer and immediately transferred to the measurement glovebox in a few minutes. The radius of the tip is expected to be ∼50 nm after metal coating. No significant change in the spring constant of the tip was found after the metal coating. Template-stripped flat metal substrates were used to grow high-quality SAMs for sample characterization and reproducible electrical measurements. The preparation of the Ag, Au, and Pt template-stripped flat substrates was described earlier.[44]

Monolayer Growth and Characterization. SAMs were formed by immersing clean template-stripped flat metal substrates in ethanol solution of molecules at a concentration of ∼0.05 mM for 20 h. The SAMs on Ag substrates were prepared in a N_2-filled glovebox. We characterized the SAMs using spectroscopic AFM, ellipsometry, and X-ray photoelectron spectroscopy (XPS). The roughness of the OPDs on template-stripped flat substrates is about 0.5 nm. Ellipsometry measurements were carried out on a VASE spectroscopic ellipsometer (J.A. Woolam Co., Inc.). The thickness of OPD monolayers on Ag, Au, and Pt obtained from

ellipsometry is shown in Figure S3. Since OPD4 was synthesized in our group, XPS was carried out to verify the adsorption of OPD4 on Ag, Au, and Pt and, the S 2p core-level data are shown in the Supporting Information (Figure S4). UV−visible absorption spectra were acquired to determine the optical HOMO−LUMO gap on OPDs in ethanol solution (Figure S5).

Work Function Measurements. SKPM measurements were used to determine the work function without (Φ) and with a SAM adsorbed on the metal surface ($\Phi_{SAM} = \Phi + \Delta\Phi$). SKPM measurements to acquire the surface potential of the samples were carried out using the same instrument that was employed for $I-V$ characterization. The AFM instrument is placed in an Ar-filled glovebox (H_2O, $O_2 < 0.1$ ppm). The typical surface potential image and histogram are shown in Figure S6. The work functions of the samples were referenced to the UPS value of OPD1 on a Au substrate.[44]

Transport Measurements. The experimental setup for electronic transport (tunneling) measurements was similar to that described in ref 35. The measurements (Figure 1) were completed by mounting the substrates in the AFM and bringing the metal-coated tip into contact with the SAM under ~1 nN of applied compressive load. Voltages were applied to the tip with a Keithley model 236 electrometer operated in "DC mode". Voltage was swept at the tip, the sample was grounded, and current−voltage characteristics were recorded; $V > 0$ means positive voltage on the tip. All measured $I-V$ curves gradually switch from practically linear at low biases to gradually more nonlinear at higher biases. The inverse of the slope of the linear portion of the $I-V$ characteristic was used to define a junction (low-bias) resistance R. The tunneling efficiency parameter β and contact resistance R_c could be extracted reproducibly from plots of the low-bias resistance *versus* molecule length. We measured the low-bias resistance between ±0.1 V in this study, and sweeps to ±1−2 V were applied to determine the transition voltage V_t and to observe the pronounced nonlinear ($I-V$) behavior.

Quantum Chemical Calculations. To understand the experimental results reported in this paper, we performed accurate *ab initio* quantum chemical calculations for all oligophenylene dithiol molecules employed (OPD1−OPD4) to fabricate the CP-AFM junctions investigated here. To treat all these molecular species at the same level of theory, we employed aug-cc-pVDZ basis sets for the C, S, and H atoms and the cc-pVDZ-PP basis set[104] for metal atoms. DFT/B3LYP calculations using Gaussian 09[105] have been carried out for geometry optimization. Ionization energies have been computed within the equation-of-motion coupled-cluster singles and doubles (EOM-IP-CCSD) method,[42,43] which represents the state-of-the-art of quantum chemistry for the molecular sizes considered. As an important technical remark, it is worth emphasizing that, although we have performed many-body EOM-IP-CCSD quantum chemical calculations at a high level of accuracy that go substantially beyond single-particle (Hartree−Fock or DFT) descriptions and used the corresponding (accurate) values of the first ionization energy, to facilitate understanding, we refer to this quantity as the HOMO energy with reversed sign. The quantum chemical calculations performed here have enabled us to microscopically validate the Newns−Anderson model that forms the basis of the present description. This contrasts to other phenomenological models of nonresonant tunneling, that could not be justified microscopically and failed to describe the data in OPD-based junctions (cf. ref 106).

Conflict of Interest: The authors declare no competing financial interest.

Supporting Information Available: Experimental and theoretical details, supplementary tables and figures. The Supporting Information is available free of charge on the ACS Publications website at DOI: 10.1021/acsnano.5b01629.

Acknowledgment. I.B. thanks Shachar Klaiman for help in calculations with CFOUR and the Deutsche Forschungsgemeinschaft (Grant BA 1799/2-1) for financial support. C.D.F. acknowledges financial support from the U.S. National Science Foundation (CHE-1213876).

REFERENCES AND NOTES

1. Reed, M. A.; Zhou, C.; Muller, C. J.; Burgin, T. P.; Tour, J. M. Conductance of a Molecular Junction. *Science* **1997**, *278*, 252–254.
2. Cui, X. D.; Primak, A.; Zarate, X.; Tomfohr, J.; Sankey, O. F.; Moore, A. L.; Moore, T. A.; Gust, D.; Harris, G.; Lindsay, S. M. Reproducible Measurement of Single-Molecule Conductivity. *Science* **2001**, *294*, 571–574.
3. Liang, W.; Shores, M. P.; Bockrath, M.; Long, J. R.; Park, H. Kondo Resonance in a Single-Molecule Transistor. *Nature* **2002**, *417*, 725–729.
4. Park, J.; Pasupathy, A. N.; Goldsmith, J. I.; Chang, C.; Yaish, Y.; Petta, J. R.; Rinkoski, M.; Sethna, J. P.; Abruna, H. D.; McEuen, P. L.; et al. Coulomb Blockade and the Kondo Effect in Single-Atom Transistors. *Nature* **2002**, *417*, 722–725.
5. Choi, S. H.; Kim, B.; Frisbie, C. D. Electrical Resistance of Long Conjugated Molecular Wires. *Science* **2008**, *320*, 1482–1486.
6. Venkataraman, L.; Klare, J. E.; Nuckolls, C.; Hybertsen, M. S.; Steigerwald, M. L. Dependence of Single-Molecule Junction Conductance on Molecular Conformation. *Nature* **2006**, *442*, 904–907.
7. Díez-Pérez, I.; Hihath, J.; Lee, Y.; Yu, L.; Adamska, L.; Kozhushner, M. A.; Oleynik, I. I.; Tao, N. J. Rectification and Stability of a Single Molecular Diode with Controlled Orientation. *Nat. Chem.* **2009**, *1*, 635–641.
8. Tao, N. J. Electron Transport in Molecular Junctions. *Nat. Nanotechnol.* **2006**, *1*, 173–181.
9. Lindsay, S. M.; Ratner, M. A. Molecular Transport Junctions: Clearing Mists. *Adv. Mater.* **2007**, *19*, 23–31.
10. McCreery, R. L.; Bergren, A. J. Progress with Molecular Electronic Junctions: Meeting Experimental Challenges in Design and Fabrication. *Adv. Mater.* **2009**, *21*, 4303–4322.
11. Salomon, A.; Cahen, D.; Lindsay, S.; Tomfohr, J.; Engelkes, V. B.; Frisbie, C. D. Comparison of Electronic Transport Measurements on Organic Molecules. *Adv. Mater.* **2003**, *15*, 1881–1890.
12. Chen, F.; Hihath, J.; Huang, Z.; Li, X.; Tao, N. J. Measurement of Single-Molecule Conductance. *Annu. Rev. Phys. Chem.* **2007**, *58*, 535–564.
13. Guo, X.; Small, J. P.; Klare, J. E.; Wang, Y.; Purewal, M. S.; Tam, I. W.; Hong, B. H.; Caldwell, R.; Huang, L.; O'Brien, S.; et al. Covalently Bridging Gaps in Single-Walled Carbon Nanotubes with Conducting Molecules. *Science* **2006**, *311*, 356–359.
14. Selzer, Y.; Salomon, A.; Cahen, D. Effect of Molecule-Metal Electronic Coupling on through-Bond Hole Tunneling across Metal-Organic Monolayer-Semiconductor Junctions. *J. Am. Chem. Soc.* **2002**, *124*, 2886–2887.
15. Nitzan, A. Electron Transmission Through Molecules and Molecular Interfaces. *Annu. Rev. Phys. Chem.* **2001**, *52*, 681–750.
16. Nitzan, A.; Ratner, M. A. Electron Transport in Molecular Wire Junctions. *Science* **2003**, *300*, 1384–1389.
17. Bumm, L. A.; Arnold, J. J.; Cygan, M. T.; Dunbar, T. D.; Burgin, T. P.; Jones, L., II; Allara, D. L.; Tour, J. M.; Weiss, P. S. Are Single Molecular Wires Conducting?. *Science* **1996**, *271*, 1705–1707.
18. Chen, J.; Reed, M. A.; Rawlett, A. M.; Tour, J. M. Large On-Off Ratios and Negative Differential Resistance in a Molecular Electronic Device. *Science* **1999**, *286*, 1550–1552.
19. Guédon, C. M.; Valkenier, H.; Markussen, T.; Thygesen, K. S.; Hummelen, J. C.; van der Molen, S. J. Observation of Quantum Interference in Molecular Charge Transport. *Nat. Nanotechnol.* **2012**, *7*, 305–309.
20. Nijhuis, C. A.; Reus, W. F.; Whitesides, G. M. Molecular Rectification in Metal-SAM-Metal Oxide-Metal Junctions. *J. Am. Chem. Soc.* **2009**, *131*, 17814–17827.
21. Reus, W. F.; Thuo, M. M.; Shapiro, N. D.; Nijhuis, C. A.; Whitesides, G. M. The SAM, Not the Electrodes, Dominates Charge Transport in Metal-Monolayer//Ga_2O_3/Gallium-Indium Eutectic Junctions. *ACS Nano* **2012**, *6*, 4806–4822.

22. Di Ventra, M.; Pantelides, S. T.; Lang, N. D. First-Principles Calculation of Transport Properties of a Molecular Device. *Phys. Rev. Lett.* **2000**, *84*, 979–982.
23. Kamenetska, M.; Koentopp, M.; Whalley, A. C.; Park, Y. S.; Steigerwald, M. L.; Nuckolls, C.; Hybertsen, M. S.; Venkataraman, L. Formation and Evolution of Single-Molecule Junctions. *Phys. Rev. Lett.* **2009**, *102*, 126803.
24. Kamenetska, M.; Quek, S. Y.; Whalley, A. C.; Steigerwald, M. L.; Choi, H. J.; Louie, S. G.; Nuckolls, C.; Hybertsen, M. S.; Neaton, J. B.; Venkataraman, L. Conductance and Geometry of Pyridine-Linked Single-Molecule Junctions. *J. Am. Chem. Soc.* **2010**, *132*, 6817–6821.
25. Parker, S. M.; Smeu, M.; Franco, I.; Ratner, M. A.; Seideman, T. Molecular Junctions: Can Pulling Influence Optical Controllability?. *Nano Lett.* **2014**, *14*, 4587–4591.
26. Seminario, J. M.; Zacarias, A. G.; Tour, J. M. Theoretical Study of a Molecular Resonant Tunneling Diode. *J. Am. Chem. Soc.* **2000**, *122*, 3015–3020.
27. Torres, R. A.; Lovell, T.; Noodleman, L.; Case, D. A. Density Functional and Reduction Potential Calculations of Fe4S4 Clusters. *J. Am. Chem. Soc.* **2003**, *125*, 1923–1936.
28. Van Dyck, C.; Geskin, V.; Kronemeijer, A. J.; de Leeuw, D. M.; Cornil, J. Impact of Derivatization on Electron Transmission through Dithienylethene-Based Photoswitches in Molecular Junctions. *Phys. Chem. Chem. Phys.* **2013**, *15*, 4392–4404.
29. Van Dyck, C.; Geskin, V.; Cornil, J. Fermi Level Pinning and Orbital Polarization Effects in Molecular Junctions: The Role of Metal Induced Gap States. *Adv. Funct. Mater.* **2014**, *24*, 6154–6165.
30. Peng, G.; Strange, M.; Thygesen, K. S.; Mavrikakis, M. Conductance of Conjugated Molecular Wires: Length Dependence, Anchoring Groups, and Band Alignment. *J. Phys. Chem. C* **2009**, *113*, 20967–20973.
31. Jones, R. O.; Gunnarsson, O. The Density Functional Formalism, Its Applications and Prospects. *Rev. Mod. Phys.* **1989**, *61*, 689–746.
32. Bâldea, I. Transition Voltage Spectroscopy Reveals Significant Solvent Effects on Molecular Transport and Settles an Important Issue in Bipyridine-Based Junctions. *Nanoscale* **2013**, *5*, 9222–9230.
33. Cuevas, J. C.; Scheer, E. *Molecular Electronics: An Introduction to Theory and Experiment*; World Scientific Publishers: River Edge, NJ, 2010.
34. Simmons, J. G. Generalized Formula for the Electric Tunnel Effect between Similar Electrodes Separated by a Thin Insulating Film. *J. Appl. Phys.* **1963**, *34*, 1793–1803.
35. Engelkes, V. B.; Beebe, J. M.; Frisbie, C. D. Length-Dependent Transport in Molecular Junctions Based on SAMs of Alkanethiols and Alkanedithiols: Effect of Metal Work Function and Applied Bias on Tunneling Efficiency and Contact Resistance. *J. Am. Chem. Soc.* **2004**, *126*, 14287–14296.
36. Holmlin, R. E.; Haag, R.; Chabinyc, M. L.; Ismagilov, R. F.; Cohen, A. E.; Terfort, A.; Rampi, M. A.; Whitesides, G. M. Electron Transport through Thin Organic Films in Metal-Insulator-Metal Junctions Based on Self-Assembled Monolayers. *J. Am. Chem. Soc.* **2001**, *123*, 5075–5085.
37. Wang, W.; Lee, T.; Reed, M. A. Mechanism of Electron Conduction in Self-Assembled Alkanethiol Monolayer Devices. *Phys. Rev. B: Condens. Matter Mater. Phys.* **2003**, *68*, 035416.
38. Vilan, A. Analyzing Molecular Current-Voltage Characteristics with the Simmons Tunneling Model: Scaling and Linearization. *J. Phys. Chem. C* **2007**, *111*, 4431–4444.
39. Holmlin, R. E.; Ismagilov, R. F.; Haag, R.; Mujica, V.; Ratner, M. A.; Rampi, M. A.; Whitesides, G. M. Correlating Electron Transport and Molecular Structure in Organic Thin Films. *Angew. Chem., Int. Ed.* **2001**, *40*, 2316–2320.
40. Bâldea, I. Transition Voltage Spectroscopy in Vacuum Break Junction: Possible Role of Surface States. *EPL (Europhys. Lett.)* **2012**, *98*, 17010.
41. Muscat, J. P.; Newns, D. M. Chemisorption on Metals. *Prog. Surf. Sci.* **1978**, *9*, 1–43.
42. Stanton, J. F.; Bartlett, R. J. The Equation of Motion Coupled-Cluster Method. A Systematic Biorthogonal Approach to Molecular Excitation Energies, Transition Probabilities, and Excited State Properties. *J. Chem. Phys.* **1993**, *98*, 7029–7039.
43. Stanton, J. F.; Gauss, J. Analytic Energy Derivatives for Ionized States Described by the Equation-of-Motion Coupled Cluster Method. *J. Chem. Phys.* **1994**, *101*, 8938–8944.
44. Kim, B.; Choi, S. H.; Zhu, X.-Y.; Frisbie, C. D. Molecular Tunnel Junctions Based on on Π-Conjugated Oligoacene Thiols and Dithiols between Ag, Au, and Pt Contacts: Effect of Surface Linking Group and Metal Work Function. *J. Am. Chem. Soc.* **2011**, *133*, 19864–19877.
45. Bâldea, I. Revealing Molecular Orbital Gating by Transition Voltage Spectroscopy. *Chem. Phys.* **2010**, *377*, 15–20.
46. Bâldea, I. Effects of Stochastic Fluctuations at Molecule–electrode Contacts in Transition Voltage Spectroscopy. *Chem. Phys.* **2012**, *400*, 65–71.
47. Bâldea, I. Ambipolar Transition Voltage Spectroscopy: Analytical Results and Experimental Agreement. *Phys. Rev. B: Condens. Matter Mater. Phys.* **2012**, *85*, 035442.
48. Bâldea, I. Interpretation of Stochastic Events in Single-Molecule Measurements of Conductance and Transition Voltage Spectroscopy. *J. Am. Chem. Soc.* **2012**, *134*, 7958–7962.
49. Beebe, J. M.; Kim, B.; Gadzuk, J. W.; Frisbie, C. D.; Kushmerick, J. G. Transition from Direct Tunneling to Field Emission in Metal-Molecule-Metal Junctions. *Phys. Rev. Lett.* **2006**, *97*, 026801.
50. Beebe, J. M.; Kim, B.; Frisbie, C. D.; Kushmerick, J. G. Measuring Relative Barrier Heights in Molecular Electronic Junctions with Transition Voltage Spectroscopy. *ACS Nano* **2008**, *2*, 827–832.
51. Bâldea, I. Single-Molecule Junctions Based on Bipyridine: Impact of an Unusual Reorganization on Charge Transport. *J. Phys. Chem. C* **2014**, *118*, 8676–8684.
52. Kim, B.; Beebe, J. M.; Jun, Y.; Zhu, X.-Y.; Frisbie, C. D. Correlation between HOMO Alignment and Contact Resistance in Molecular Junctions: Aromatic Thiols versus Aromatic Isocyanides. *J. Am. Chem. Soc.* **2006**, *128*, 4970–4971.
53. Wold, D. J.; Frisbie, C. D. Formation of Metal-Molecule-Metal Tunnel Junctions: Microcontacts to Alkanethiol Monolayers with a Conducting AFM Tip. *J. Am. Chem. Soc.* **2000**, *122*, 2970–2971.
54. Wold, D. J.; Frisbie, C. D. Fabrication and Characterization of Metal-Molecule-Metal Junctions by Conducting Probe Atomic Force Microscopy. *J. Am. Chem. Soc.* **2001**, *123*, 5549–5556.
55. Beebe, J. M.; Engelkes, V. B.; Miller, L. L.; Frisbie, C. D. Contact Resistance in Metal-Molecule-Metal Junctions Based on Aliphatic SAMs: Effects of Surface Linker and Metal Work Function. *J. Am. Chem. Soc.* **2002**, *124*, 11268–11269.
56. Song, H.; Kim, Y.; Jang, Y. H.; Jeong, H.; Reed, M. A.; Lee, T. Observation of Molecular Orbital Gating. *Nature* **2009**, *462*, 1039–1043.
57. Guo, S.; Hihath, J.; Díez-Pérez, I.; Tao, N. J. Measurement and Statistical Analysis of Single-Molecule Current-Voltage Characteristics, Transition Voltage Spectroscopy, and Tunneling Barrier Height. *J. Am. Chem. Soc.* **2011**, *133*, 19189–19197.
58. Guo, S.; Zhou, G.; Tao, N. J. Single Molecule Conductance, Thermopower, and Transition Voltage. *Nano Lett.* **2013**, *13*, 4326–4332.
59. Mishchenko, A.; Vonlanthen, D.; Meded, V.; Bürkle, M.; Li, C.; Pobelov, I. V.; Bagrets, A.; Viljas, J. K.; Pauly, F.; Evers, F.; et al. Influence of Conformation on Conductance of Biphenyl-Dithiol Single-Molecule Contacts. *Nano Lett.* **2010**, *10*, 156–163.
60. Xiao, X.; Xu, B.; Tao, N. J. Measurement of Single Molecule Conductance: Benzenedithiol and Benzenedimethanethiol. *Nano Lett.* **2004**, *4*, 267–271.

61. Kronemeijer, A. J.; Huisman, E. H.; Akkerman, H. B.; Goossens, A. M.; Katsouras, I.; van Hal, P. A.; Geuns, T. C. T.; van der Molen, S. J.; Blom, P. W. M.; de Leeuw, D. M. Electrical Characteristics of Conjugated Self-Assembled Monolayers in Large-Area Molecular Junctions. *Appl. Phys. Lett.* **2010**, *97*, 173302.
62. Kronemeijer, A. J.; Katsouras, I.; Huisman, E. H.; van Hal, P. A.; Geuns, T. C. T.; Blom, P. W. M.; de Leeuw, D. M. Universal Scaling of the Charge Transport in Large-Area Molecular Junctions. *Small* **2011**, *7*, 1593–1598.
63. Kondo, M.; Tada, T.; Yoshizawa, K. Wire-Length Dependence of the Conductance of Oligo(p-Phenylene) Dithiolate Wires: A Consideration from Molecular Orbitals. *J. Phys. Chem. A* **2004**, *108*, 9143–9149.
64. Pauly, F.; Viljas, J. K.; Cuevas, J. C. Length-Dependent Conductance and Thermopower in Single-Molecule Junctions of Dithiolated Oligophenylene Derivatives: A Density Functional Study. *Phys. Rev. B: Condens. Matter Mater. Phys.* **2008**, *78*, 035315.
65. Cohen, R.; Stokbro, K.; Martin, J. M. L.; Ratner, M. A. Charge Transport in Conjugated Aromatic Molecular Junctions: Molecular Conjugation and Molecule-Electrode Coupling. *J. Phys. Chem. C* **2007**, *111*, 14893–14902.
66. Sayed, S. Y.; Fereiro, J. A.; Yan, H.; McCreery, R. L.; Bergren, A. J. Charge Transport in Molecular Electronic Junctions: Compression of the Molecular Tunnel Barrier in the Strong Coupling Regime. *Proc. Natl. Acad. Sci. U. S. A.* **2012**, *109*, 11498–11503.
67. Alloway, D. M.; Hofmann, M.; Smith, D. L.; Gruhn, N. E.; Graham, A. L.; Colorado, R.; Wysocki, V. H.; Lee, T. R.; Lee, P. A.; Armstrong, N. R. Interface Dipoles Arising from Self-Assembled Monolayers on Gold: UV - Photoemission Studies of Alkanethiols and Partially Fluorinated Alkanethiols. *J. Phys. Chem. B* **2003**, *107*, 11690–11699.
68. Alloway, D. M.; Graham, A. L.; Yang, X.; Mudalige, A.; Colorado, R.; Wysocki, V. H.; Pemberton, J. E.; Lee, T. R.; Wysocki, R. J.; Armstrong, N. R. Tuning the Effective Work Function of Gold and Silver Using ω -Functionalized Alkanethiols: Varying Surface Composition through Dilution and Choice of Terminal Groups. *J. Phys. Chem. C* **2009**, *113*, 20328–20334.
69. Bâldea, I. Important Insight into Electron Transfer in Single-Molecule Junctions Based on Redox Metalloproteins from Transition Voltage Spectroscopy. *J. Phys. Chem. C* **2013**, *117*, 25798–25804.
70. Schmickler, W. A Theory of Adiabatic Electron-Transfer Reactions. *J. Electroanal. Chem. Interfacial Electrochem.* **1986**, *204*, 31–43.
71. Bâldea, I. Extending the Newns-Anderson Model to Allow Nanotransport Studies through Molecules with Floppy Degrees of Freedom. *EPL (Europhys. Lett.)* **2012**, *99*, 47002.
72. Bâldea, I.; Köppel, H.; Wenzel, W. (4,4′)-Bipyridine in Vacuo and in Solvents: A Quantum Chemical Study of a Prototypical Floppy Molecule from a Molecular Transport Perspective. *Phys. Chem. Chem. Phys.* **2013**, *15*, 1918–1928.
73. Zahid, F.; Paulsson, M.; Datta, S. Electrical Conduction through Molecules. In *Advanced Semiconductors and Organic Nano-Techniques*; Morkoç, H., Ed.; Elsevier: New York, 2003; Vol. 3, Electrical Conduction through Molecules chapter.
74. Heimel, G.; Romaner, L.; Brédas, J.-L.; Zojer, E. Interface Energetics and Level Alignment at Covalent Metal-Molecule Junctions: Π-Conjugated Thiols on Gold. *Phys. Rev. Lett.* **2006**, *96*, 196806.
75. Heimel, G.; Romaner, L.; Zojer, E.; Brédas, J.-L. Toward Control of the Metal-Organic Interfacial Electronic Structure in Molecular Electronics: A First-Principles Study on Self-Assembled Monolayers of Π-Conjugated Molecules on Noble Metals. *Nano Lett.* **2007**, *7*, 932–940.
76. Koch, N.; Duhm, S.; Rabe, J. P.; Vollmer, A.; Johnson, R. L. Optimized Hole Injection with Strong Electron Acceptors at Organic-Metal Interfaces. *Phys. Rev. Lett.* **2005**, *95*, 237601.
77. Xie, Z. T.; Ding, B. F.; Gao, X. D.; You, Y. T.; Sun, Z. Y.; Zhang, W. H.; Ding, X. M.; Hou, X. Y. Photoemission Study of C_{60}-Induced Barrier Reduction for Hole Injection at N, N′-Bis(naphthalene-1-y1)-N, N′-Bis(phenyl) benzidine/Al. *J. Appl. Phys.* **2009**, *105*, 106105.
78. Zehner, R. W.; Parsons, B. F.; Hsung, R. P.; Sita, L. R. Tuning the Work Function of Gold with Self-Assembled Monolayers Derived from X-$[C_6H_4$-C≡C-$]_nC_6H_4$-SH (N = 0, 1, 2; X = H, F, CH_3, CF_3, and OCH_3). *Langmuir* **1999**, *15*, 1121–1127.
79. Choi, S. H.; Risko, C.; Delgado, M. C. R.; Kim, B.; Brédas, J.-L.; Frisbie, C. D. Transition from Tunneling to Hopping Transport in Long, Conjugated Oligo-Imine Wires Connected to Metals. *J. Am. Chem. Soc.* **2010**, *132*, 4358–4368.
80. Luo, L.; Choi, S. H.; Frisbie, C. D. Probing Hopping Conduction in Conjugated Molecular Wires Connected to Metal Electrodes. *Chem. Mater.* **2011**, *23*, 631–645.
81. Hines, T.; Diez-Perez, I.; Hihath, J.; Liu, H.; Wang, Z. S.; Zhao, J.; Zhou, G.; Müllen, K.; Tao, N. Transition from Tunneling to Hopping in Single Molecular Junctions by Measuring Length and Temperature Dependence. *J. Am. Chem. Soc.* **2010**, *132*, 11658–11664.
82. Kim, T.; Vázquez, H.; Hybertsen, M. S.; Venkataraman, L. Conductance of Molecular Junctions Formed with Silver Electrodes. *Nano Lett.* **2013**, *13*, 3358–3364.
83. Huang, M.-J.; Hsu, L.-Y.; Fu, M.-D.; Chuang, S.-T.; Tien, F.-W.; Chen, C.-H. Conductance of Tailored Molecular Segments: A Rudimentary Assessment by Landauer Formulation. *J. Am. Chem. Soc.* **2014**, *136*, 1832–1841.
84. Wold, D. J.; Haag, R.; Rampi, M. A.; Frisbie, C. D. Distance Dependence of Electron Tunneling through Self-Assembled Monolayers Measured by Conducting Probe Atomic Force Microscopy: Unsaturated versus Saturated Molecular Junctions. *J. Phys. Chem. B* **2002**, *106*, 2813–2816.
85. Bâldea, I. A Quantum Chemical Study from a Molecular Perspective: Ionization and Electron Attachment Energies for Species Often Used to Fabricate Single-Molecule Junctions. *Faraday Discuss.* **2014**, *174*, 37–56.
86. Tan, A.; Balachandran, J.; Dunietz, B. D.; Jang, S.-Y.; Gavini, V.; Reddy, P. Length Dependence of Frontier Orbital Alignment in Aromatic Molecular Junctions. *Appl. Phys. Lett.* **2012**, *101*, 243107.
87. Fracasso, D.; Muglali, M. I.; Rohwerder, M.; Terfort, A.; Chiechi, R. C. Influence of an Atom in EGaIn/Ga_2O_3 Tunneling Junctions Comprising Self-Assembled Monolayers. *J. Phys. Chem. C* **2013**, *117*, 11367–11376.
88. Markussen, T.; Chen, J.; Thygesen, K. S. Improving Transition Voltage Spectroscopy of Molecular Junctions. *Phys. Rev. B: Condens. Matter Mater. Phys.* **2011**, *83*, 155407.
89. Smaali, K.; Clément, N.; Patriarche, G.; Vuillaume, D. Conductance Statistics from a Large Array of Sub-10 nm Molecular Junctions. *ACS Nano* **2012**, *6*, 4639–4647.
90. Tran, T. K.; Smaali, K.; Hardouin, M.; Bricaud, Q.; Oçafrain, M.; Blanchard, P.; Lenfant, S.; Godey, S.; Roncali, J.; Vuillaume, D. A Crown-Ether Loop-Derivatized Oligothiophene Doubly Attached on Gold Surface as Cation-Binding Switchable Molecular Junction. *Adv. Mater.* **2013**, *25*, 427–431.
91. Huisman, E. H.; Guédon, C. M.; van Wees, B. J.; van der Molen, S. J. Interpretation of Transition Voltage Spectroscopy. *Nano Lett.* **2009**, *9*, 3909–3913.
92. Araidai, M.; Tsukada, M. Theoretical Calculations of Electron Transport in Molecular Junctions: Inflection Behavior in Fowler-Nordheim Plot and Its Origin. *Phys. Rev. B: Condens. Matter Mater. Phys.* **2010**, *81*, 235114.
93. Bâldea, I.; Xie, Z.; Frisbie, C. D. Uncovering a Law of Corresponding States for Electron Tunneling in Molecular Junctions. *Nanoscale* **2015**, *7*, 10465–10471.
94. Cahen, D.; Kahn, A. Electron Energetics at Surfaces and Interfaces: Concepts and Experiments. *Adv. Mater.* **2003**, *15*, 271–277.
95. Hwang, J.; Wan, A.; Kahn, A. Energetics of Metal-Organic Interfaces: New Experiments and Assessment of the Field. *Mater. Sci. Eng., R* **2009**, *64*, 1–31.

96. Braun, S.; Salaneck, W. R.; Fahlman, M. Energy-Level Alignment at Organic/metal and Organic/organic Interfaces. *Adv. Mater.* **2009**, *21*, 1450–1472.
97. Salomon, A.; Boecking, T.; Seitz, O.; Markus, T.; Amy, F.; Chan, C.; Zhao, W.; Cahen, D.; Kahn, A. What Is the Barrier for Tunneling Through Alkyl Monolayers? Results from N- and P-Si−Alkyl/Hg Junctions. *Adv. Mater.* **2007**, *19*, 445–450.
98. Meir, Y.; Wingreen, N. S. Landauer Formula for the Current through an Interacting Electron Region. *Phys. Rev. Lett.* **1992**, *68*, 2512–2516.
99. Salem, L. *The Molecular Orbital Theory of Conjugated Systems*; W.A. Benjamin: New York, 1966.
100. Sun, X.; Gobbi, M.; Bedoya-Pinto, A.; Txoperena, O.; Golmar, F.; Llopis, R.; Chuvilin, A.; Casanova, F.; Hueso, L. E. Room-Temperature Air-Stable Spin Transport in Bathocuproine-Based Spin Valves. *Nat. Commun.* **2013**, *4*, 2794.
101. Song, H.; Reed, M. A.; Lee, T. Single Molecule Electronic Devices. *Adv. Mater.* **2011**, *23*, 1583–1608.
102. Wang, G.; Kim, T.-W.; Jo, G.; Lee, T. Enhancement of Field Emission Transport by Molecular Tilt Configuration in Metal-Molecule-Metal Junctions. *J. Am. Chem. Soc.* **2009**, *131*, 5980–5985.
103. DiBenedetto, S. A.; Facchetti, A.; Ratner, M. A.; Marks, T. J. Charge Conduction and Breakdown Mechanisms in Self-Assembled Nanodielectrics. *J. Am. Chem. Soc.* **2009**, *131*, 7158–7168.
104. Peterson, K. A.; Puzzarini, C. Systematically Convergent Basis Sets for Transition Metals. II. Pseudopotential-Based Correlation Consistent Basis Sets for the Group 11 (Cu, Ag, Au) and 12 (Zn, Cd, Hg) Elements. *Theor. Chem. Acc.* **2005**, *114*, 283–296.
105. Frisch, M. J.; Trucks, G. W.; Schlegel, H. B.; Scuseria, G. E.; Robb, M. A.; Cheeseman, J. R.; Scalmani, G.; Barone, V.; Mennucci, B.; Petersson, G. A.; et al. *Gaussian 09*; Gaussian Inc.: Wallingford, CT, 2010.
106. Bâldea, I. Important issues facing model-based approaches to tunneling transport in molecular junctions. *Phys. Chem. Chem. Phys.* **2015**, Advanced Article, DOI: 10.1039/C5CP02595H.